ELSEVIER

Journal of Luminescence 72–74 (1997) 12–17

JOURNAL OF LUMINESCENCE

Far- and near-field optical spectroscopy of cleaved edge quantum wires

M. Katz[a], D. Gershoni[a,*], T.D. Harris[b], L.N. Pfeiffer[b]

[a] Physics Department, Technion-Israel Institute of Technology, Haifa, 32000, Israel

[b] Lucent Technologies Bell Laboratories, Murray Hill, NJ 07974, USA

Abstract

We used low-temperature continuous wave and time-resolved optical spectroscopy together with near-field scanning optical microscopy for the studies of multiple and single, nanometer dimension, cleaved edge overgrown strained quantum wires. We measured the radiative lifetime, polarization selection rules and absorption strength of the cleaved edge quantum wells and quantum wires and compared between them. Our experimental results are discussed in terms of the relevant theories.

Keywords: Optical selection rules; Excitons; Near-field optical microscopy; 1D systems

1. Introduction

Among the most promising ways to achieve quantum confinement in more than one direction is cleaved edge overgrowth (CEO) [1]. This technique utilizes several orthogonal directions of epitaxial growth, exploiting the precision of layer thickness control to form uniform intersecting planes of semiconductor. In this work we describe optical studies of strained layer quantum wires in which confinement to 1D is produced by one-dimensional pseudomorphic strain [2]. This strain is induced in the (1 1 0) oriented CEO quantum well (QW) by a (1 0 0) oriented strained layer QW. The lateral dimensions of quantum wires (QWRs) produced by this technique are comparable to the dimensions of the intersecting layers from which they are formed. Thus truly nanometer scale QWRs are obtained.

2. Samples

Two samples different only in their first growth stage were used for this study. In the first sample, a 150 periods of 7 nm thick layer of $In_{0.07}Ga_{0.93}As$ followed by 21 nm thick layer of GaAs were epitaxially grown on a (1 0 0) oriented GaAs substrate. The strained layer superlattice (SLS) was capped by a 2 μm thick GaAs layer. For the second sample five strained $In_{0.10}Ga_{0.90}As$ QWs of 30, 15, 7.5, 3.8, and 1.8 nm, respectively, were grown on a (1 0 0) oriented GaAs substrate. The strained QWs, were separated by 1.0 μm thick layers of GaAs and capped by a 2 μm thick GaAs layer. Both samples were then thinned, scribed, and mounted in a molecular beam epitaxy (MBE) machine. They were cleaved during growth, exposing thus a (1 1 0) facet, onto which the following layers were grown in succession: 20 nm $Al_{0.3}Ga_{0.7}As$, 8 nm GaAs, 20 nm $Al_{0.3}Ga_{0.7}As$, 3.5 nm GaAs, 20 nm $Al_{0.3}Ga_{0.7}As$, and 5 nm GaAs. This way an array of 300 strained QWRs (SQWRs) was formed on the cleaved edge of

* Corresponding author.

0022-2313/97/$17.00 Published by Elsevier Science B.V.
PII S0022-2313(97)00086-0

the first sample, while a set of 10 single SQWRs was formed on the cleaved edge of the second sample. The first sample was used for the far field optical studies, and the second one was used for the near-field optical studies.

3. Far-field studies

In Fig. 1(a) and (b) we display the continuous wave (CW) far-field photoluminescence (PL) and the linearly polarized PL excitation (PLE) of the 8 nm CEO QW. (8 nm × 7 nm SQWR array). For these measurements, light from a CW Ti:sapphire laser was focused at normal incidence to a spot of roughly 3 μm diameter on the (1 1 0) CEO facet of the sample using a ×60 microscope objective mounted in the He-flow cryostat. The emitted light was collected by the same objective and it was analyzed by a 0.25 m double monochromator and a cooled photomultiplier.

In order to facilitate an experimental comparison between the emission from the SQWRs and that of the QWs, a few μm change in the microscope objective position was needed, while everything else remain unchanged. Two PLE spectra are shown for the QW and the SQWR. The dashed and solid PLE curves were obtained with incident polarization parallel ($1\bar{1}0$ direction) and perpendicular to the wires (0 0 1 direction), respectively. The PL peaks are Stokes shifted from the lowest energy excitonic resonances observed in the PLE measurements. These Stokes shifts, typically of the order of the PL line width at low temperature, and their temperature dependence are comparable in both the QWs and the SQWRs. The assignments of excitonic transitions in the PLE spectra are marked in Fig. 1(a). The numbers refer to the conduction band sublevel, the valence band sublevel and the letter $H(L)$ indicates that this is a heavy (light) hole subband. These sublevels result from confinement in the (1 1 0) direction, and the observed transitions agree to within 3 MeV with the calculated ones [3,4]. In marked contrast to the unpolarized PLE of a conventional (1 0 0) QW, the (1 1 0) QWs show clear polarization dependence [4]. The light hole (LH) transitions are preferably linearly polarized along the (0 0 1) direction and the heavy hole (HH)

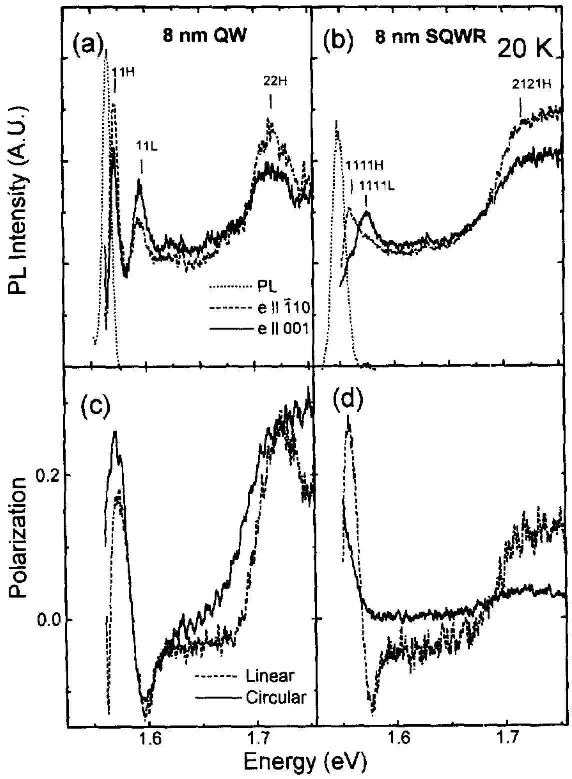

Fig. 1. PL and polarized PLE spectra of the CEO QW (a and c) and SQWRs (b and d).

transitions along the ($1\bar{1}0$) direction. In Fig. 1(b) additional quantum numbers are added to the conduction and valence sublevels to indicate the confinement in the (0 0 1) direction. The HH transitions in the PLE of the SQWR are red shifted ~17 meV relative to the corresponding QW transitions, while the LH transitions are red shifted by as much as 27 meV. This is a consequence of the strain induced potential change and the lateral confinement [2, 3].

The linear and circular polarization spectra of the QW (SQWRs) are given in Fig. 1(c) (Fig. 1(d)). Extreme changes are observed in the transition intensities and linear polarization anisotropy of the SQWRs compared to this of the unstrained QW. We first note that the LH of the transition of the SQWR is stronger than the HH one, in clear contrast with the unstrained QW. Second, the degree of linear polarization of the SQWRs is larger than that of the QW. This is in agreement with our model calculations [3,4].

The situation is reversed in the circular polarization spectrum. Here while the HH QW excitons are positively (parallel) polarized and the LH excitons are negatively (crossed) polarized as expected for a QW [5]. The SQWRs excitons are completely unpolarized due to the added mixture of the excitonic wave function by the strained lateral perturbation.

For the PL decay time measurements light from a picosecond pulsed Ti:Sapphire laser was used. The PL was detected by a multichannel plate photomultiplier. For the analysis of the measured temporal transients [6], a single exponential decay model, convoluted with the system response function, was used. In Fig. 2(a) we plot on a logarithmic scale the temperature dependence of the PL decay times from the 8 nm QW by open circles and that from the associated QWR by solid circles. It is seen that at this temperature range (10–90 K) the decay times follow roughly a temperature power-law dependence. The decay times from the QWs increase almost linearly with temperature, as demonstrated by the dashed line of slope 1 which is drawn through the measured points. The temperature dependence of the lifetimes of the QW is in clear contrast with the decay times from the QWRs. Here the solid lines of slope $\frac{1}{2}$ describe the temperature dependence of the decay times much better. In particular, we note that as a result of this difference in the temperature dependence, the decay times of the PL from the QWRs become shorter than those from the corresponding QWs above a certain temperature. This is a clear demonstration of the different densities of states of the two quantum systems. In the 2D QW, the density of thermalized exciton states is roughly energy independent, whereas in the 1D QWR it is roughly inversely proportional to the square root of the exciton kinetic energy [7].

While the PL decay time measures the excitonic radiative and nonradiative population lifetime, the PL emission intensity immediately after the excitation pulse measures the excitonic radiative decay time only. This is because the intensity of the emission is proportional to the excitonic radiative decay rate. In Fig. 2(b) we plot the temperature dependence of the PL intensity integrated over the first

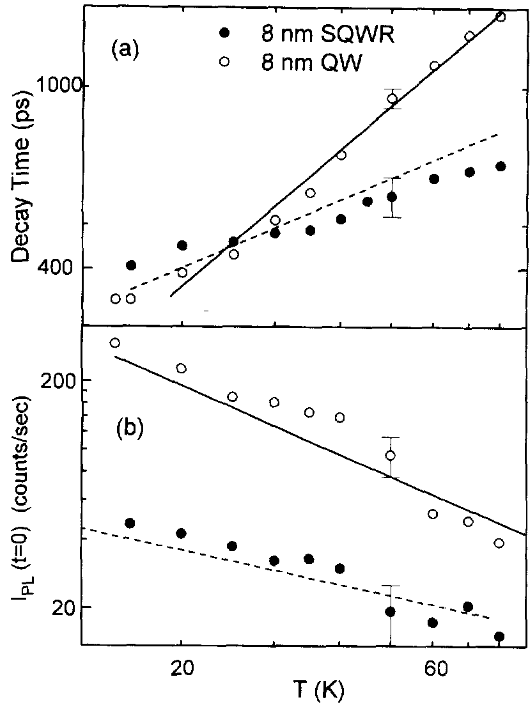

Fig. 2. Log–log plot of the CEO QW and SQWR PL decay time (a) and PL intensity immediately after the excitation pulse (b) as a function of the sample temperature.

100 ps immediately after the excitation pulse ended. The PL intensity from the QW is almost inversely proportional to the temperature, as demonstrated by the dashed lines of slope -1 which is drawn through the measured points. Whereas the temperature dependence of the PL emission intensity from the SQWRs is roughly inversely proportional to the square root of the temperature as demonstrated by the solid line of slope $-\frac{1}{2}$. This demonstrates most clearly that the measured decay times at this temperature range is mostly radiative in both quantum systems.

4. Near-field studies

In order to compare between the excitonic absorption cross section of the 1D and 2D systems one needs to study a single QWR. Heterogeneity and carrier and electromagnetic field interactions between neighboring wires are eliminated this way. The probed volume of the QW is orders of magnitude larger than the probed volume of a QWR if far-field optics is used. Instead, we use the enhanced spatial resolution of low-temperature near-field scanning optical microscopy (LT-NSOM) for this task.

The low-temperature NSOM microscope used for this study is described in detail elsewhere [8]. All the data reported here used excitation and collection with the same aluminum coated, tapered fiber probe at a sample temperature of 4 K.

Two modes of data acquisition were used: PL spectral images are generated by fixing the excitation energy and recording a PL spectrum for 1–5 s at each tip position, using a cooled CCD array detector. Alternately, at a single tip position PL intensity integrated over a selected spectral range is recorded as a function of the excitation energy.

In Fig. 3 we show four selective wavelength PL images associated with the spectral lines of four of the single SQWRs and the CEO QW [9]. The images were generated from 441 near-field PL spectra obtained from a 21×21 pixel scan of a 2.5 μm × 2.5 μm square region of the second CEO sample. The integration spectral interval is indicated above each image. These images allow an accurate determination of the spatial source of each spectral feature. The positions of the underlying (1 0 0) oriented strained 1.8, 3.8, 7.5 and 15 nm InGaAs QWs, are marked on the images by the bold dashed lines. These positions were identified by similar selective wavelength images integrated over the PL lines of those QWs [9]. Image No. 1 is obtained by integrating over the PL from the CEO 8 nm QW. The image clearly shows that the spatial origin of this emission strongly anti-correlates with the positions of the strained QWs, peaking between them. The other three images are obtained by integrating over longer wavelength ranges. The fixed

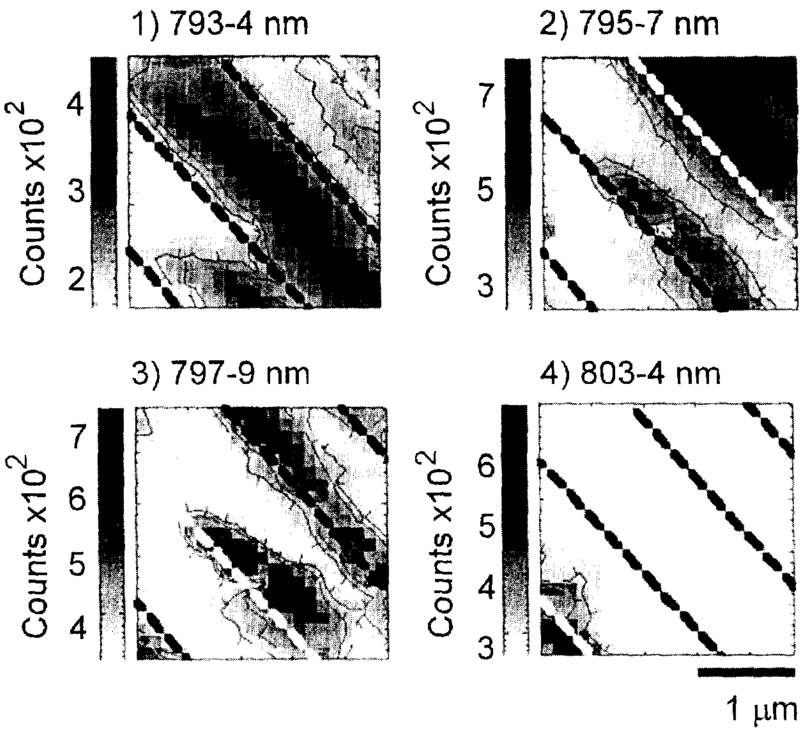

Fig. 3. LT-NSOM selective wavelength PL images of the CEO single SQWRs sample.

wavelength images of these spectral lines strongly correlate with the spatial position of the (1 0 0) oriented strained InGaAs QWs. There can be no doubt that the strain field of the underlying (1 0 0) InGaAs layers perturbs the (1 1 0) GaAs QW and shifts its emission to lower energy relative to the emission from the unperturbed QW. This perturbation, affects the semiconductor band structure only directly above the strained InGaAs QWs, and thus along a very well-defined direction in the (1 1 0) oriented QW plane. This direction defines the SQWR where carriers are confined to narrow stripes within the (1 1 0) oriented GaAs QW plane. As expected, the magnitude of the spectral red shift scales with the width of the strained layer which determines the dimension of the lateral confinement [3]. We noted that the PL images clearly indicate that the emission from the QWs and QWRs originate from fully (OD) localized centers at this temperature [10].

In Fig. 4 we show the PL (solid line) and PLE (dashed line) spectra of the 15 nm SQWR as obtained by the LT-NSOM. when its tip was parked above this SQWR (image No. 4 in Fig. 3). Since the NSOM tip, ~300 nm in diameter a factor of 20 larger than the SQWR, carrier diffusion from the well to the wire cannot be avoided. Consequently, all the spectral features associated with QW absorption are seen in the PLE spectrum of the SQWR. The spectral feature centered at 799 nm in the PLE spectrum of the SQWR is at a lower energy than the QW band edge and thus can only be assigned to SQWR absorption. We assume that all photo-generated carriers up to a tip radius diffuse to recombine in the SQWR. This assumption is supported by the images of Fig. 3. There is negligible emission from the QW when the tip is positioned directly over a QWR. Since the magnitudes of PL emission from the SQWRs and the QW are comparable, non-radiative recombination can be reasonably ignored. Thus, the ratio of QW and QWR absorption cross section can be estimated by comparing the peak area of the lowest-energy transition of the QW to that of the SQWR, correcting for the geometric area of the two structures. The QW to SQWR area ratio under the tip is approximately 20:1, while the QW–QWR PLE intensity ratio is roughly 6:1 as determined by the two

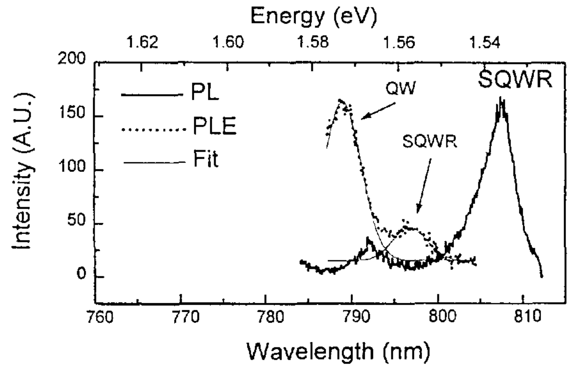

Fig. 4. Near-field PL and PLE spectra of the CEO 15 nm × 8 nm SQWR.

Gaussians model fit to the data shown in Fig. 4. A factor of 3 enhancement in the absorption cross section of the wire with respect to that of the well is thus determined. This result is in agreement with theoretical estimations [11].

5. Conclusions

We used far- and near-field optical spectroscopies to compare between a cleaved edge QW to a cleaved edge QWR. We observed marked differences between the two systems in their optical transition energies, linear and circular polarization selection rules, PL decay times, spectral shape and absorption cross section. These are a direct consequence of the different dimensionality of the two systems.

References

[1] L.N. Pfeiffer, K.W. West, H.L. Stormer, J. Eisenstein, K.W. Baldwin, D. Gershoni and J. Spector, Appl. Phys. Lett. 56 (1990) 1697.

[2] D. Gershoni, J.S. Weiner, S.N.G. Chu, G.A. Baraff, J.M. Vandenberg, L.N. Pfeiffer, K.W. West, R.A. Logan and T. Tanbun-Ek. Phys. Rev. Lett. 65 (1990) 1631.

[3] G.A. Baraff and D. Gershoni, Phys. Rev. B 43 (1991) 4011.

[4] D. Gershoni, I. Brener, G.A. Baraff, S.N.G. Chu, L.N. Pfeiffer and K. West, Phys. Rev. B 44 (1991) 1931.

[5] C. Weisbuch, R.C. Miller, R. Dingle, A.C. Gossard and W. Wiegmann, Sol. Stat. Comm. 37 (1981) 219.

[6] D. Gershoni, M. Katz, W. Wegscheider, L.N. Pfeiffer, R.A. Logan and K.W. West, Phys. Rev. B 50 (1994) 8930.
[7] D.S. Citrin, Phys. Rev. Lett. 69 (1992) 3393.
[8] R.D. Grober, T.D. Harris, J.K. Trautman and E. Betzig, Rev. Sci. Instr. 65, 626.
[9] T.D. Harris, D. Gershoni, R.D. Grober, L.N. Pfeiffer, K.W. West and N. Chand, Appl. Phys. Lett. 68 (1966) 988.
[10] H.F. Hess, E. Betzig, T.D. Harris, L.N. Pfeiffer and K.W. West, Science 264 (1994) 1740.
[11] I. Suemune and L.A. Coldren, IEEE J. QE. 24 (1988) 1778.